IL NUOVO CIMENTO Vol. 25 C, N. 2 Marzo-Aprile 2002

Evolution of nocturnal temperature inversions: A numerical study(*)

S. Ragothaman([1]), R. Narasimha([2])(**) and A. S. Vasudeva Murthy([3])

([1]) *Department of Earth Sciences, Meteorology, Uppsala University - Uppsala, Sweden*
([2]) *Jawaharlal Nehru Centre for Advanced Scientific Research - Bangalore 560094, India*
([3]) *TIFR Centre, Indian Institute of Science Campus - Bangalore 560012, India*

(ricevuto il 13 Gennaio 2000; revisionato il 10 Agosto 2001; approvato il 18 Settembre 2001)

Summary. — A series of numerical simulations using a one-dimensional energy balance model suggest that both the depth and the intensity of the nocturnal temperature inversion depend on surface emissivity ϵ_g and a ground cooling rate parameter β (which in the model is a surrogate for the inverse square root of the soil thermal diffusivity), especially under calm conditions. It is found that, after a transient that may last a few hours after nominal sunset, both depth and intensity follow the classical parabolic growth law, but only under calm conditions. If the ground cools faster the transient for the inversion depth is longer and the inversion deeper. If the surface is radiatively darker, the transient is again longer but the inversion depth is lower. The temperature at the top of the inversion is not strongly influenced by ϵ_g or β, but, depending on whether the reference is taken at the surface or at screen height, the intensity of the inversion decreases (or increases) with a drop in ϵ_g; it also increases with increase in ground cooling rate but with either choice of reference temperature. With wind, the inversion may be deeper during the transient than under calm conditions, but eventually becomes both shallower and weaker, and may disappear altogether at high winds. The effect of wind is found to be negligible when the friction velocity is less than 0.2 $\mathrm{m\,s^{-1}}$. Comparison with observations shows general qualitative agreement, but also suggests that the highly variable results reported in the literature on inversion parameters may be due to site-dependent surface characteristics whose effects, till now ignored, need explicit attention in future field observations and models.

PACS 92.60.Fm – Boundary layer structure and processes.
PACS 47.70.-n – Reactive, radiative, or nonequilibrium flows.

(*) The authors of this paper have agreed to not receive the proofs for correction.
(**) Also at the National Institute of Advanced Studies, Indian Institute of Science Campus Bangalore 560012, India. E-mail:roddam@caos.iisc.ernet.in

1. – Introduction

Temperature inversions are among the most significant features of the stable nocturnal boundary layer; an example of their practical importance is their role in the suppression of the dispersion of pollutants or in the formation of fog in the atmosphere. However, the present understanding of the dynamics of nocturnal inversions is rather incomplete, and any advance there may be expected to improve our ability to model the nocturnal boundary layer, which itself still remains poorly understood (*e.g.* [1]). It is therefore no surprise that nocturnal inversions are receiving increasing attention in the last few decades.

In this paper, the results of a series of numerical simulations of the nocturnal inversion are presented. A model due to Vasudeva Murthy, Srinivasan and Narasimha [2] (hereafter VSN) has been used for this purpose; the primary aim is to examine the influence of surface parameters—in particular ground emissivity and surface cooling rate—on major inversion parameters such as depth and intensity (as measured by appropriate temperature differences across the inversion layer). Figure 1 is a schematic that defines these parameters and shows two typical temperature profiles under study; the one showing a lifted temperature minimum has been studied in detail elsewhere ([2, 3] and references cited therein). In general, the parameters of special interest in the temperature distribution are the inversion height z_{inv} and the associated temperature differences

$$\Delta T_{\mathrm{inv}} = T_{z_{\mathrm{inv}}} - T_g, \quad \Delta T_s = T_{z_{\mathrm{inv}}} - T_s,$$

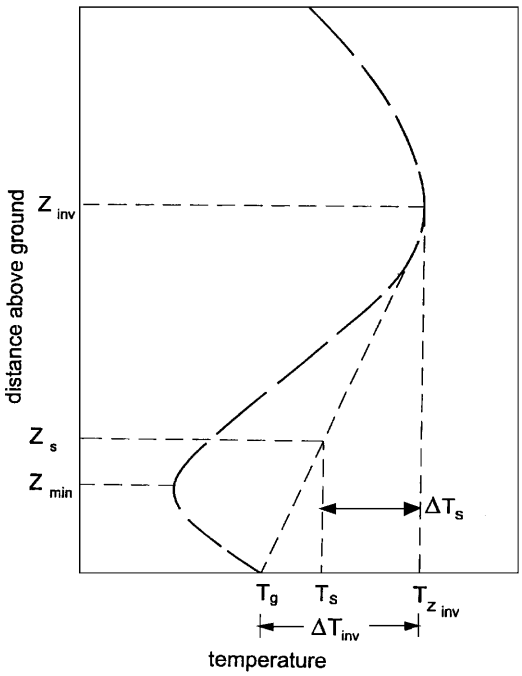

Fig. 1. – Schematic of two typical nocturnal temperature distributions with radiation inversion, showing notation adopted. The distribution on left shows a "lifted minimum" at z_{min}.

where T_g is the temperature of the ground, T_s is the temperature at the screen height z_s (assumed to be 1.22 m), and $T_{z_{\rm inv}}$ is the temperature at $z_{\rm inv}$. A second aim of the study is to examine the nature of the evolution of inversion layer parameters, especially with regard to the prevalence of parabolic growth or the $\sqrt{t}$ law (t being time), proposed long ago by Taylor [4] and still often used (*e.g.* [5]). The present study is a continuation of the simulations being carried out by the authors to understand the role of radiation in nocturnal boundary layers [3, 6].

As fig. 1 includes the possiblity of a lifted temperature minimum, it may be worthwhile to touch upon the role of the phenomenon in the present study. In the first place it must be realized that a lifted minimum can occur due to several different reasons. One reason could be advection from cooler areas (say with vegetation). Fleagle and Badgley [7] have observed it over the oceans, and Lettau [8] over snow in Antarctica. Oke [9] reports lifted minima over both bare soil and a surface covered with grass, and has argued that the mechanism operating to produce what is known as the "grass tip minimum" is different from that over bare soil. The careful work of Raschke [10] has established beyond doubt that a lifted minimum can occur even over bare soil in the absence of winds (and hence also of advection). It is the occurrence of the phenomenon over bare soil that has presented the greatest puzzle. For the sake of simplicity, and to emphasize the basic physics of the problem, the VSN model was formulated only for a bare soil surface; the present study is also restricted to such surfaces. The modelling of exchange processes over a surface covered with vegetation is more complicated and not yet fully understood (see, for example, Jacobs *et al.* [11]). It must however be emphasized that this paper is not directly concerned with the lifted temperature minimum; under certain conditions it occurs automatically in the present simulations, but when it does it is usually so close to the surface that its occurrence is not central to the results that we present here on inversion parameters.

Many aspects of the nocturnal inversion have been examined by various workers. Such studies include Nieuwstadt [12], who provides a rate equation for the inversion height; Garratt and Brost [13], who use a simplified second-order closure model of the boundary layer evolution to calculate longwave radiative flux divergence; Andre and Mahrt [14], who have analysed data from the Wangara and Voves experiments; and Mahrt *et al.* [15], who have carried out an observational study of the nocturnal boundary layer. However all these investigations are silent on the effect of surface parameters. Indeed it is sometimes explicitly asserted (*e.g.* [14]) that surface emissivity effects can be supposed to be negligible beyond a few meters from the ground. However, it is not very difficult to think of situations where radiation is the dominant mechanism in the nocturnal boundary layer (for example, under very low wind conditions); the influence of the underlying surface on the temperature distribution at large heights above ground may not necessarily be negligible under such conditions, in the light of the studies reported by VSN [2, 3], and needs to be investigated in detail.

There are several studies that concentrate on either pure radiation only, ignoring turbulent diffusion (*e.g.* [16-18]), or turbulent diffusion only, without radiation (*e.g.* [19-21]). But present understanding clearly indicates (*e.g.* [13, 14]) that both turbulent heat transfer as well as clear air radiative cooling need to be taken into account for a more accurate description of the development of nocturnal inversions. Hence, in the present analysis, we shall consider both these scenarios. However, we first examine radiation-dominated conditions to determine the influence of surface parameters, and then consider the effect of including eddy diffusion.

Using observational data, the prevalence or otherwise of the parabolic evolution of

the inversion height and intensity has been studied by Surridge and others [5, 22]. They provide evidence that the $\sqrt{t}$ law for the growth of the inversion layer is not always obeyed. The present simulations seek to throw light on this problem as well.

In sect. **2**, we discuss details of the VSN model and the numerical methodology used for this study. In sect. **3**, the evolution of the inversion is discussed. The influence of surface parameters is discussed in sect. **4** and the effect of eddy diffusion in sect. **5**. In sect. **6**, a comparison of the simulation results with appropriate observations is made. In the final section, conclusions from this study are outlined.

2. – Problem formulation and method of solution

The model used here is presented in detail in VSN, so we restrict ourselves to a brief description.

2˙1. *The VSN model.* – We basically consider a 1D model with no advective changes. We assume clear skies, with wind profile, surface temperature variation and the humidity of the air incorporated as parameters that can be prescribed; although the soil temperature can be independently computed through a coupled air-soil model, also formulated in VSN, we shall restrict ourselves to the approach where the ground temperature is a prescribed function of time, as this has been shown to be entirely adequate and furthermore has the advantage of providing a more immmediate physical interpretation [2]. The governing equation for the air temperature T, which is a function of vertical distance z from the surface and time t only, can then be written as the energy balance equation

$$\rho_a c_p \frac{\partial T}{\partial t} = -\frac{\partial Q}{\partial z}, \tag{1}$$

where ρ_a is the density of air, c_p is the specific heat at constant pressure and Q is the total energy flux, split into three components,

$$Q = Q_m + Q_t + Q_r, \tag{2}$$

where Q_m, Q_t and Q_r are the contributions to the energy flux from conduction, convection and long-wave radiation, respectively. The first two terms are taken to be given by diffusion,

$$Q_m = -K_m \frac{\partial T}{\partial z}, \quad Q_t = -K_t \frac{\partial \theta}{\partial z}, \quad \theta = T + \Gamma z \tag{3}$$

where K_m is the molecular conductivity of air, K_t is the eddy conductivity, θ is the potential temperature and Γ is a (prescribed) constant lapse rate. The eddy conductivity is further taken to be given by the expression

$$K_t = \rho_a c_p U_* k_* z \phi(\mathrm{Ri}) \tag{4}$$

where U_* is the friction velocity, k_* is the Karman constant and $\phi(\mathrm{Ri})$ is a stability function which, following Liou and Ou [23], is taken as

$$\begin{aligned} \phi(\mathrm{Ri}) &= 1.35(1 - 9\ \mathrm{Ri})^{-1/2} \text{ for Ri } \leq 0 \\ &= 1.35(1 + 6.35\ \mathrm{Ri})^{-1} \text{ for Ri } > 0, \end{aligned} \tag{5}$$

Ri being the Richardson number

$$\mathrm{Ri} = \frac{k_*^2 g z^2}{U_*^2 \theta} \frac{\partial \theta}{\partial z}. \tag{6}$$

VSN discuss in some detail the reasons behind the choice of this particular way of modelling Q_t.

The radiative flux Q_r is given by

$$Q_r = F^{\uparrow} - F^{\downarrow}, \tag{7}$$

where $F^{\uparrow}$ and $F^{\downarrow}$ are the upward and downward radiative fluxes, respectively. They are modelled using the broad-band flux emissivity method [23, 24], which gives

$$F^{\downarrow} = \int_u^{u_\infty} \sigma T^4(u', t) \frac{\mathrm{d}\epsilon(u' - u)}{\mathrm{d}u'} \mathrm{d}u', \tag{8}$$

$$F^{\uparrow} = \{\epsilon_g \sigma T_g^4(t) + (1 - \epsilon_g) F^{\downarrow}(0)\}\{1 - \epsilon(u)\} - \int_0^u \sigma T^4(u', t) \frac{\mathrm{d}\epsilon(u - u')}{\mathrm{d}u'} \mathrm{d}u', \tag{9}$$

where σ is the Stefan-Boltzmann constant and u is the water vapour mass path length given by

$$u(z) = \int_0^z \rho_w(z') \left\{ \frac{p(z')}{p(0)} \right\}^{\delta} \mathrm{d}z', \tag{10}$$

$\rho_w(z)$ denotes the density of water vapour at level z, $p(z)$ denotes the pressure of air at level z and $u_\infty = u(\infty)$ is the total atmospheric path length. (Primes on symbols in the above integrals denote dummy variables of integration.) The exponent δ is chosen to be 0.9, following Garratt and Brost [13]; ϵ_g is the ground emissivity, $T_g(t)$ is the ground temperature and $\epsilon(u)$ is the broad-band flux emissivity function of water vapour, taken here as

$$\begin{aligned} \epsilon(u) &= 0.0492 \ln (1 + 1263.5u) \quad \text{for} \quad u \le 10^{-2} \text{kg m}^{-2}, \\ &= 0.05624 \ln (1 + 875u) \quad \text{for} \quad u > 10^{-2} \text{kg m}^{-2}, \end{aligned} \tag{11}$$

following Zdunkowski and Johnson [25].

The boundary conditions are taken to be

$$T(z, 0) = T_{g0} - \Gamma z, \tag{12}$$

$$T(0, t) = T_{g0} - \beta \sqrt{t}, \tag{13}$$

$$\frac{\partial T}{\partial z}(\infty, t) = -\Gamma, \tag{14}$$

where β is the ground cooling rate parameter, inversely proportional to the square root of the thermal diffusivity of the soil by the well-known theory due to Brunt [2, 3]. T_{g_0} is a specified temperature of ground at a suitably defined initial instant $t = 0$. This

initial instant, which we have called "nominal" sunset [3], occurs slightly ahead of actual sunset (by a time of order about 1/2 hour or less). The time of nominal sunset as well as the parameters β and T_{g0} are best determined by fitting a $\sqrt{t}$ curve to observed ground temperature, as we have done [2] in an analysis of data from Raschke [10]. The initial condition (12), which assumes that the temperature distribution is represented by a simple linear lapse, is nominally prescribed at sunset. In actual fact it becomes valid only after a short transient around the time of sunset: it must be appreciated that the solar radiant energy flux received at the ground (per unit surface area) starts diminishing significantly rather before sunset. Correspondingly there is an evening transitional epoch over which the solutions computed here cannot be expected to be strictly valid. However the condition prescribed is realistic, as boundary layer studies suggest that the transitional epoch can be surprisingly short (*e.g.* [26]). Thus, although the instantaneous initial condition we have imposed is not strictly achieved in the atmosphere, we expect it to be realistic shortly after sunset.

2˙2. *Numerical methodology.* – The basic approach for solving the governing equation is based on the method of lines. Here eq. (1) is discretized in two stages. In the first stage, the space variable is discretized on a selected space mesh chosen *a priori* for the entire calculation, so as to convert (1) into a system of ordinary differential equations with time as the independent variable. This system is then solved using a standard software package with an appropriate discretization in time, to be discussed below. This approach is essentially the same as VSN have adopted in their earlier studies. More details about the numerical methodology can be found in Vasudeva Murthy *et al.* [27].

For the spatial discretization, the whole domain is divided into a fixed number of slabs (four in the present case: 0 to 2 m, 2 m to 20 m, 20 m to 200 m and 200 m to 1 km). Note that the slabs are of unequal height, because of the wide disparity in the gradients, and correspondingly also in the length scales characterising the temperature distributions in the problem. Within each slab a uniform mesh is chosen, with 500 points between ground and 2 m, 100 between 2 m and 20 m, 150 between 20 m and 200 m and 250 between 200 m and 1 km, making a total of 1000 points in the whole domain. Previous experience has shown that such fine resolution is necessary for accurate computations of the temperature field, especially near ground.

3. – The nature of evolution under calm conditions

Wind speed has been set to zero for the first series of simulations (*i.e.* $U_* \equiv 0$). As mentioned earlier, the prevalence or otherwise of the $\sqrt{t}$ law is examined here. For this purpose, a least-squares $\sqrt{t}$ fit is made for all the simulation results considered in this section, over that stretch of time during which the deviation of the least-squares fit from the actual simulation value, as a fraction of the latter, is less than 2%. In other words, we determine the duration over which the relative error involved in the fit is less than 2%.

Following the discussion in VSN, we consider a range of values of ϵ_g from 0.7 to 1.0 and of β from 0 to 15 $\mathrm{K\,h^{-1/2}}$.

Figure 2 shows the evolution of the inversion height and of the temperature differences across the inversion for $\epsilon_g = 0.8$ and $\beta = 2\ \mathrm{K\,h^{-1/2}}$. This case is referred to as the "baseline" case throughout this paper. It can be seen that i) the top of the inversion layer grows in proportion to the square root of the elapsed time right from about 1 h, ii) $\Delta T_{\mathrm{inv}} (= T(z_{\mathrm{inv}}, t) - T_g)$ shows $\sqrt{t}$ behaviour only from about $t = 4.5$ h and iii)

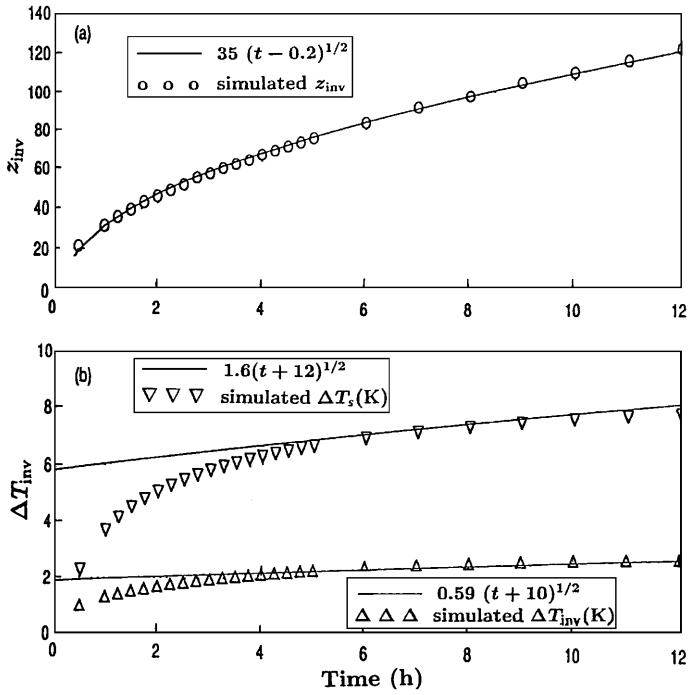

Fig. 2. – Parabolic growth of inversion parameters for the baseline case.

$\Delta T_s (= T(z_{\rm inv}) - T_s)$ shows $\sqrt{t}$ behaviour from about 5 h after the initial instant.

In order to examine this $\sqrt{t}$ behaviour further, we define an onset time t_0, which is the time after the initial instant from which the inversion parameter grows in proportion to $\sqrt{t}$.

First of all, it is seen that, in general, no unique onset time exists for all the three inversion parameters considered; indeed the variation is large, from 1 h for $z_{\rm inv}$ to 5 h for ΔT_g when $\epsilon_g = 0.8$ and $\beta = 2.0\ {\rm K\,h^{-1/2}}$.

Figure 3 shows how the onset time varies with ϵ_g and β. It can be seen that, for $z_{\rm inv}$, there is a slow increase in the value of t_0 as β is increased, and a somewhat larger increase when ϵ_g is increased. The onset time for ΔT_g varies little with ϵ_g, but drops from 5 h to 2.25 h as β is increased from 2 to 5 ${\rm K\,h^{-1/2}}$, and varies little thereafter. For ΔT_s, the onset time shows broadly similar variations although it initially increases from 3.75 h at $\epsilon_g = 0.7$ to 4.5 h for $\epsilon_g \geq 0.8$.

Hence, it is seen that during calm conditions, the inversion layer eventually thickens in proportion to the square root of elapsed time, the onset of this behaviour being delayed slightly for faster ground cooling (*i.e.* lower soil thermal diffusivity) and rather more as ground emissivity approaches unity.

For values of the ground cooling rate parameter greater than 2 ${\rm K\,h^{-1/2}}$, ΔT_g begins to show the $\sqrt{t}$ behaviour earlier than it does for the baseline case, but for high values of the ground cooling rate, as can be seen from earlier results, both $z_{\rm inv}$ as well as ΔT_g begin to obey the $\sqrt{t}$ law roughly at about the same time, namely about $t = 2.0$ h. Similar to ΔT_g, ΔT_s also begins to show the $\sqrt{t}$ behaviour earlier for higher values of the ground cooling rate. Thus, for ground cooling rates rather greater than about 2 ${\rm K\,h^{-1/2}}$ (*i.e.* for

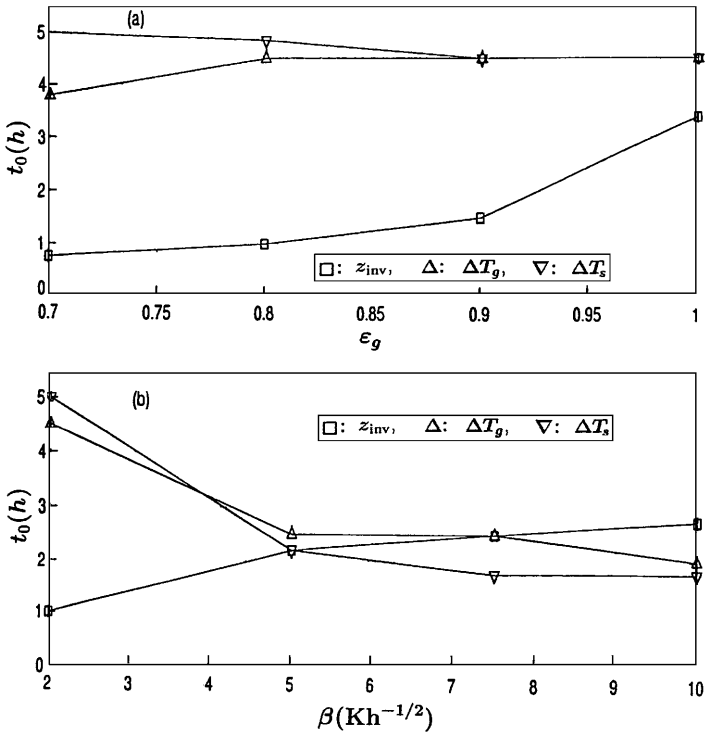

Fig. 3. – Variation of time of onset of parabolic growth in inversion parameters with ground emissivity and cooling rate.

sufficiently low soil thermal diffusivities), z_{inv}, ΔT_g as well as ΔT_s begin to show the $\sqrt{t}$ behaviour roughly at about the same time, namely $t = 2$ h from the initial instant. For $\beta = 2.0\ \mathrm{K\,h^{-1/2}}$ and different values of ϵ_g ranging from 0.7 to 1.0, the inversion height begins to obey the $\sqrt{t}$ law much earlier than ΔT_g.

Now, the rate equation for the growth of the inversion layer proposed by Nieuwstadt [12], which was discussed in sect. **1**, results in a monotonic growth of the inversion layer for the pure radiation case, as also found here. However, Nieuwstadt does not assess the validity of the $\sqrt{t}$ law, nor does he discuss the evolution of the temperature differences; he assumes a radiation profile chosen independently of the temperature distribution. We shall discuss the observational results of Surridge [5] regarding the $\sqrt{t}$ law in sect. **6**.

The present simulations confirm the expectation that the molecular diffusivity has no influence on either the inversion height or the temperature differences; detailed results are not presented here, but may be found in [6].

Let us now consider the effect of varying the mixing ratio q_0 on z_{inv} and ΔT_g. Figure 4 shows the evolution of z_{inv} for $q_0 = 0.01$ and $q_0 = 0.001$. It can be seen that z_{inv} at large times is increased very marginally by a ten-fold rise in q_0. Similarly, ΔT_g at large times is reduced very marginally by the same rise in q_0 (fig. 4). In view of the results of VSN, it is not surprising that the effect of q_0 is confined to the lowest metre or so of the atmosphere, and at greater heights the effect of mixing ratio is negligible.

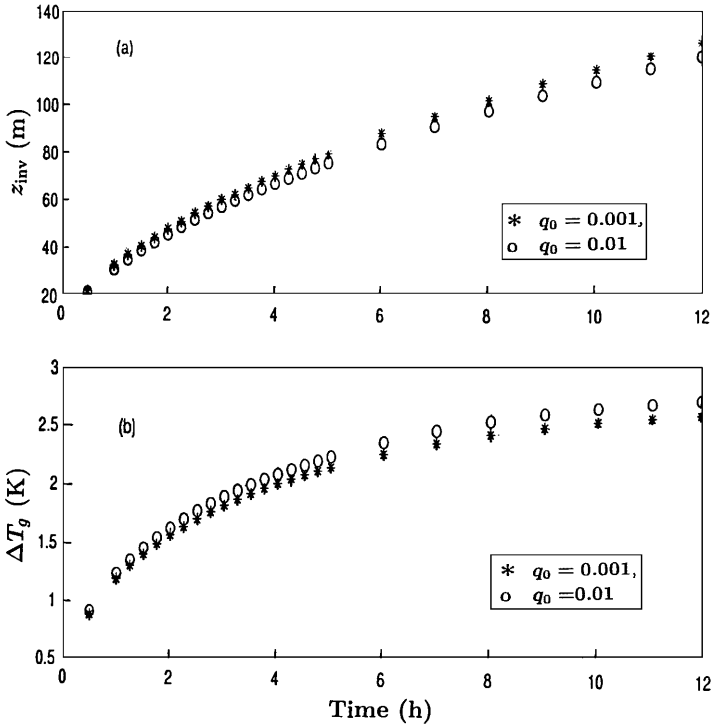

Fig. 4. – Effect of moisture on the evolution of inversion height.

4. – Surface influence under radiation-dominated conditions

We now investigate the effect of varying ϵ_g and β on the inversion height as well as the temperature differences across the inversion. For these simulations also the wind speed is set to zero, in order to obtain radiation-dominated conditions. It can be seen from fig. 5 that $z_{\rm inv}$ is higher for higher values of β. For example, when β is increased from 2 K $\rm h^{-1/2}$ to 10 K $\rm h^{-1/2}$, the inversion height, say at 11 h, increases from about 115 m to about 175 m, that is by more than 50 %. Hence, higher the cooling rate, deeper is the inversion.

Figure 5 also shows that $z_{\rm inv}$ decreases as the ground emissivity is increased; for example, as ϵ_g increases from 0.7 to 1.0 the inversion height, at say 11 h, decreases from 130 m to 70 m, that is by about 45%. The reason for this is to be found in the effect of ϵ_g on radiative cooling rates. It has been shown by detailed flux-emissivity and band models [28, 29] that, as ϵ_g drops from 1.0 to 0.8, the cooling rate *increases*, dramatically at heights of 1 m or less, but significantly even upto a height of about 1 km. The increase in cooling rate is due to the term $(1-\epsilon_g)F^{\downarrow}(0)$ in eq. (9); loosely speaking, $F^{\downarrow}(0)$ carries the characteristics of the lower temperatures at higher altitudes. The higher cooling rate increases the depth of the inversion under radiation-dominated conditions.

Let us now consider the effect of surface properties on the temperature differences. Figure 6 shows the evolution of ΔT_g for four values of ϵ_g, namely 0.7, 0.8, 0.9 and 1.0. It can be seen that when ϵ_g is increased from 0.7 to 1.0, ΔT_g at 11 h increases from 2.4 K to 3.7 K (about 55%). When β is increased from 2 to 5 K $\rm h^{-1/2}$, ΔT_g at 11 h increases

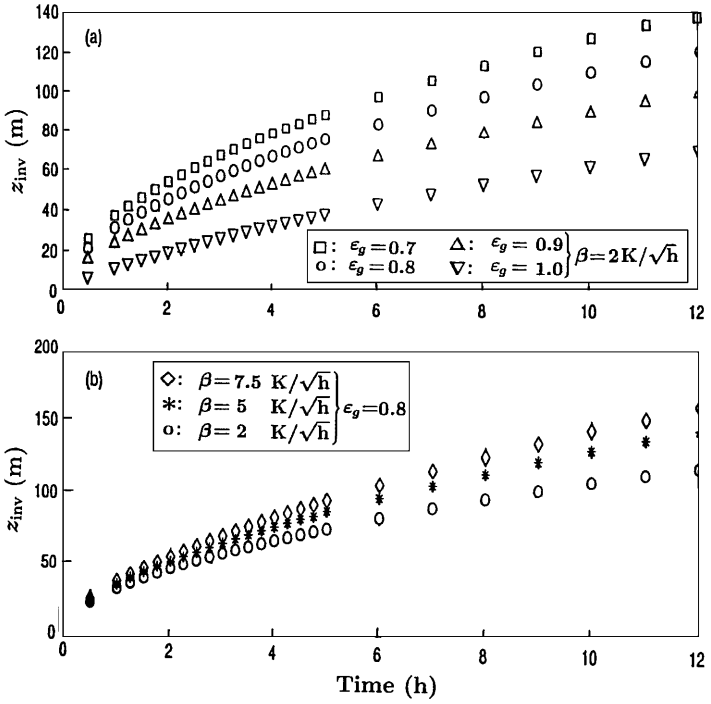

Fig. 5. – Effect of surface emissivity and cooling rate on the evolution of the inversion depth.

dramatically from about 2.5 K to about 12 K. However, this enormous increase is largely due to low ground temperatures: while T_g falls by about 10 degrees (from 293.4 to 283.4 K), $T_{\rm inv}$ changes only by 0.4 degrees (from 295.9 to 283.4 K).

Let us now consider the difference ΔT_s. Figure 7 shows that ΔT_s *decreases* with increase in ϵ_g, unlike ΔT_g. For example, when ϵ_g is increased from 0.7 to 1.0, ΔT_s say at 11 h decreases from about 11 K to about 2.8 K; that is by about 72%. It may at first seem surprising that ΔT_g and ΔT_s change in opposite directions as ϵ_g is varied. However the reason is simply that the temperature distribution between ground and screen height can change dramatically with changes in ground emissivity, as the results of [3] show.

Figure 7 also shows that ΔT_s increases with β, like ΔT_g but less strongly. For example, when β is increased from 2 to 5 K h$^{-1/2}$, ΔT_s at 11 h increases from 8 K to about 12 K, that is by 50%, unlike ΔT_g which increases five-fold for the same increase in β. Once again, it is clear that the enormous increase in ΔT_g with β must largely be attributed to the lower ground temperature.

We recall that the results discussed so far correspond to the pure radiation case. However, they can be considered to hold good, at least qualitatively, for low wind speeds also. Hence, under such conditions, it is seen that a lower ground emissivity leads to a deeper inversion, and a decrease in ΔT_g but increase in ΔT_s. A higher surface cooling rate also results in a deeper inversion, but has opposite effects on the temperature differences; ΔT_g is higher (largely because ground is cooler), but ΔT_s, which is a more representative indicator of inversion intensity, is appreciably lower.

Further, it must be noted from figs. 6 and 7 that for higher ground emissivities and cooling rates, the evolution of ΔT_g and ΔT_s is more or less similar. This is a clear

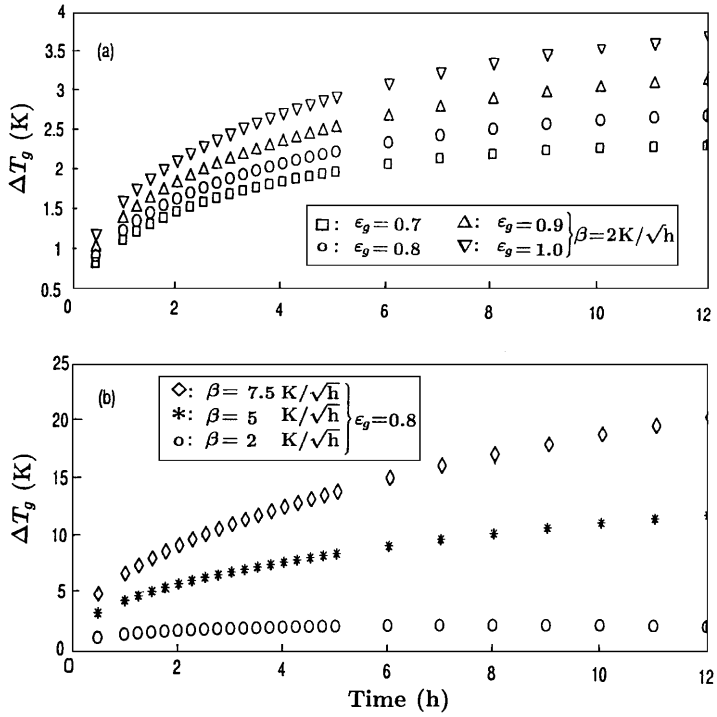

Fig. 6. – Effect of surface emissivity and cooling rate on the evolution of the temperature difference ΔT_g.

indication of the ground conditions in which ΔT_s can be taken as a surrogate for ΔT_g. For lower ϵ_g and β, this is not the case.

Finally, the assumption of calm conditions, while certainly frequently relevant to the tropics, will not always obtain in reality. It therefore needs to be determined upto what value of friction velocity the assumption of effectively calm conditions is valid. Furthermore there will be ranges of U_* values over which both eddy diffusion and radiation will be significant (see [14]). Well above this range eddy diffusion plays the dominant role. We now consider situations where both mechanisms have significant roles to play.

5. – Effect of eddy diffusion

Here, we consider situations where eddy diffusion cannot be neglected. For these numerical experiments we have used U_* values that lie within the range 0.01–1 $\mathrm{m\,s^{-1}}$. First let us consider the evolution for moderate values of U_*, namely 0.1 and 0.2 $\mathrm{m\,s^{-1}}$, which we shall call the "low-wind cases". Results are shown in fig. 8 along with the evolution under calm conditions. It can be seen that upto a little more than 1 h, the inversion height under calm conditions is slightly less than the values obtained with low-wind. However, whereas the inversion height with wind begins to *decrease* after about 3 h, the inversion height for $U_* = 0$ continues to increase monotonically. Among the low-wind cases themselves, the inversion height for $U_* = 0.2\ \mathrm{m\,s^{-1}}$ is slightly higher than that for the other two cases upto 4 h and is lower thereafter. It can also be seen from

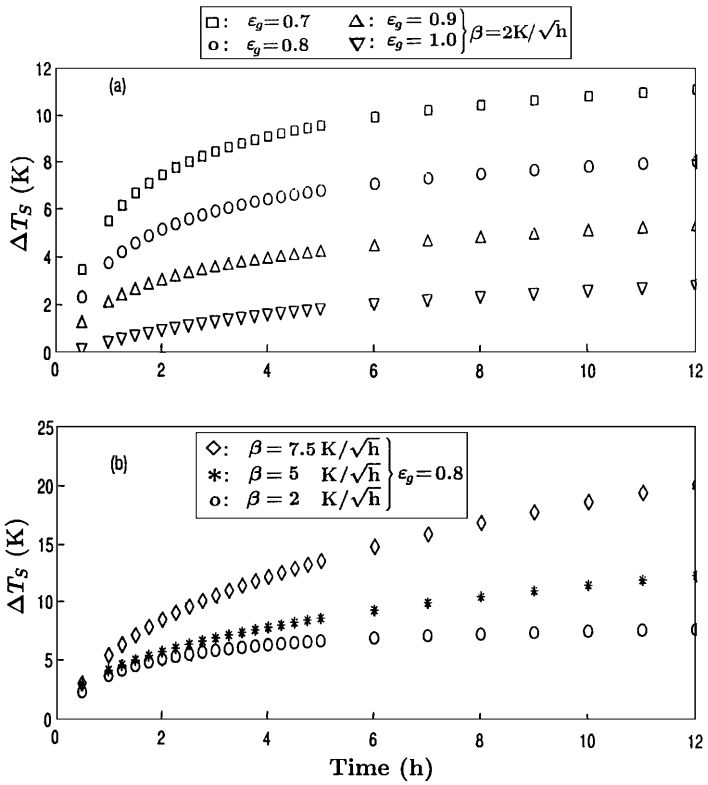

Fig. 7. – Effect of surface emissivity and cooling rate on the evolution of the temperature difference ΔT_s.

fig. 8 that values of ΔT_g obtained in the low-wind cases considered are always less than that for the $U_* = 0$ case. Also, the temperature difference with wind begins to decrease after reaching a maximum at about 2 h. At the end of 7 h, it can be seen that the inversion is about to disappear altogether. In general, ΔT_g decreases with increasing wind.

Figure 8 also shows the evolution of the inversion height for the high-wind cases, U_* = 0.5 and 1 $\mathrm{m\,s^{-1}}$, which are well above the range considered previously. It can be seen that the inversion height is further reduced, reaches a maximum in the first 2 hours and begins to decrease thereafter. Although this cannot be seen clearly in fig. 8, it turns out that ΔT_g is slightly higher for $U_* = 1\ \mathrm{m\,s^{-1}}$ than for $U_* = 0.5\ \mathrm{ms^{-1}}$ during the first 2 h, and thereafter falls below that for the latter case.

In summary, we find that eddy diffusion initially raises the inversion height above the value under calm conditions, but eventually lowers it, the cross-over time occurring earlier as U_* increases. Even when there is a shallow inversion at higher winds, it is weak, and tends to disappear some 5 h after sunset.

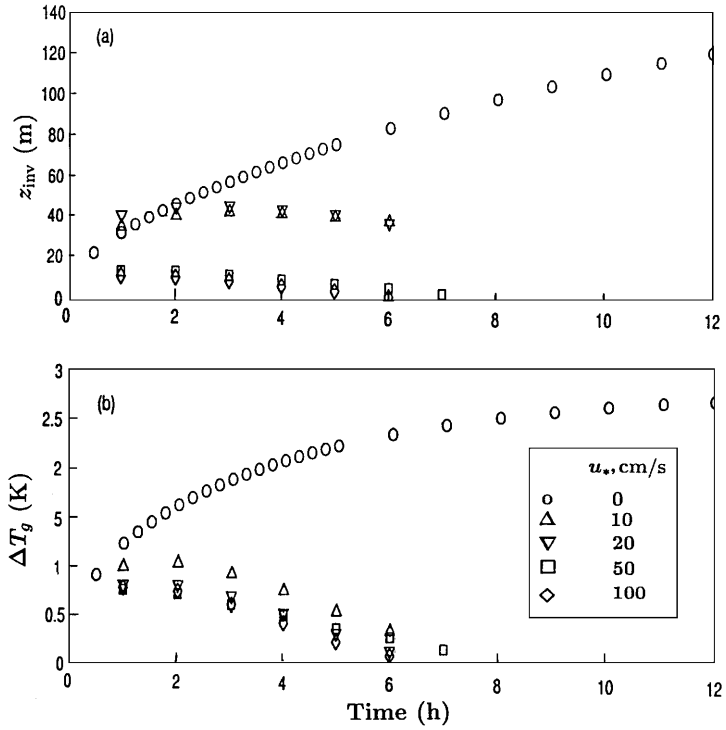

Fig. 8. – Effect of eddy diffusion on the evolution of inversion height and intensity.

6. – Comparison with observations

Here we shall compare the simulation results with observations [5, 30, 31]. As pointed out by Oke [9], the two main sources of error in measuring air temperatures are associated with poor ventilation and extraneous radiation exchanges. Both these errors can be effectively eliminated by use of fine-wire thermometers. As Ramdas [31] made his first measurements (in 1932) using Asmann aspiration psychrometers, their accuracy had been doubted, but Raschke under the suggestion of Geiger came to India from Germany (in the mid-1950's) to investigate temperature distributions near ground, using thermocouple psychrometers (having fine electrical measuring sensors) that he brought with him [10]. The small radiation errors that these sensors are subject to were compensated by a special procedure developed by him [32]. Temperatures were recorded thrice in a three-minute cycle with an accuracy of 0.1°C. In general Raschke's work [10] was carried out with extreme care.

Coming now to measurements of temperature inversions, the data have been obtained from instrumented balloons [30]; the accuracy of this technique is better than that of a radiosonde. What the present study suggests is that lack of data on basic surface parameters like ground emissivity and soil thermal conductivity may well constitute far greater sources of uncertainty in understanding inversion layer dynamics than any errors due to current observational techniques.

Indeed, the major problem in carrying out comparisons between observations and the present simulations is that the former do not include values of ϵ_g, β and wind, all of

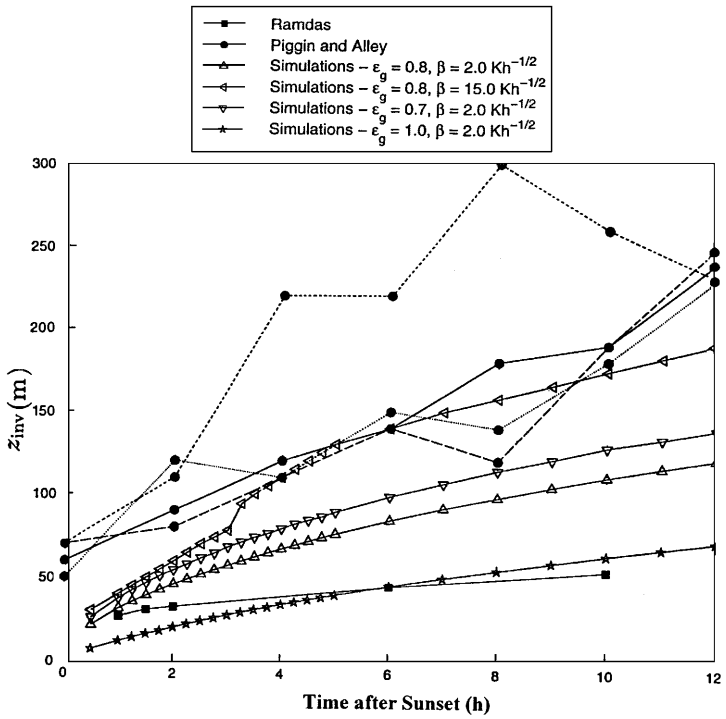

Fig. 9. – Comparison of the present simulation results with observations in India.

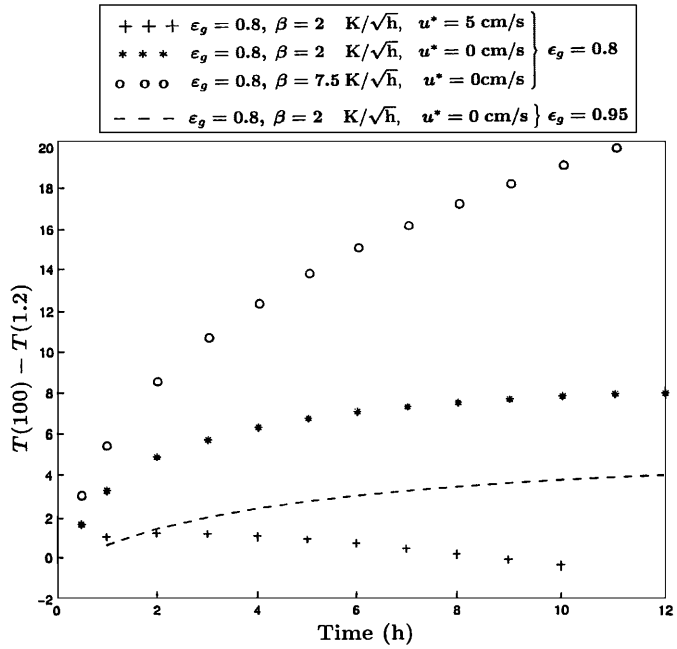

Fig. 10. – Results from present simulations at various values of cooling rate and friction velocity, showing examples of non-parabolic evolution.

which (as we have seen) exert a significant influence on inversion characteristics. Under the circumstances, we can only hope to find out whether the present simulations reproduce observations for some reasonable set of values of the *unmeasured* parameters, are broadly consistent with observed behaviour, and make predictions that lend themselves to experimental tests.

Figure 9 shows a comparison of the inversion height obtained from the present simulations with a series of four observations reported by Piggin and Alley [30], and with one set of observations reported by Ramdas [31] in Pune. The former observations were made under "light winds" (wind speed was less than about 2 $\mathrm{m\,s^{-1}}$, so we can expect $U_* = 0.2\ \mathrm{m\,s^{-1}}$ or less, which as seen in sect. **5** represents effectively calm conditions), at four sites (Bhilai, Rourkela, Durgapur and Bokaro). The simulated inversion heights were obtained using values of ϵ_g in the range 0.7–1.0 and β in the range 2–15 $\mathrm{K\,h^{-1/2}}$. It can be seen that the inversion height obtained from the simulations with $\epsilon_g = 0.8$ and $\beta = 15\ \mathrm{K\ \ h^{-1/2}}$ fall within the range of observed values in three of the four observations of [30]. The fourth set, taken at Bokaro, shows very high values of inversion height, with a suggestion of shrinking beginning 8 h after sunset. To reproduce this fourth set of observations might demand lower ϵ_g and higher β, with an occasional gust of wind; we have not attempted this as requiring inputs that are too complicated. In general, the simulation results can be considered to be not inconsistent with observations.

No information about winds is given by Ramdas [31]. The low values of inversion depth observed by him (presumably at low winds) are consistent with the predictions of our baseline case.

Let us now consider the measurements made by Surridge [5] who has observed that on some sites the temperature difference $T_{100} - T_s$, where T_{100} and T_s denote temperature at 100 m and screen height respectively, does not increase more rapidly than $\sqrt{t}$ during the initial hours and increases much more slowly later. For example in one of his observations, the aforementioned difference increased to 90% of its peak value in 2 h, which is only about 16% of the total time. These observations were made when wind speeds were less than 3 $\mathrm{m\,s^{-1}}$.

Figure 10 shows the evolution of $T_{100} - T_s$ obtained from the present simulations for calm conditions and for different values of ϵ_g and β that are indicated on the figure. It can be seen that, in general, the temperature difference increases to 50% of its peak value in 2 h. Figure 10 also shows the evolution for $\epsilon_g = 0.8$, $\beta = 2.0\ \mathrm{K\,h^{-1/2}}$ and $U_* = 0.05\ \mathrm{m\,s^{-1}}$. Here it can be seen that at 2 h the peak value of $T_{100} - T_s$ has been reached. Hence, the present model is entirely capable of simulating the non-parabolic behaviour for the difference $T_{100} - T_s$ observed by Surridge.

Finally, we consider a comparison of the inversion heights presented in the previous section with those observed during the Wangara experiments, which have been tabulated by Yu [33]. An analysis of these observations can be found in [14] and [15], which have been discussed in sect. **1**. From Yu's tables it is found that the U_* values appropriate for the Wangara nights lie in the range 0.01 to 0.27 $\mathrm{m\,s^{-1}}$. Also, on all the occasions, the inversion height is more than or equal to 100 m, except on Day 18 at 24 h and Day 33 at 18 h when it is 50 m. Moreover, on a couple of occasions on Day 44, when the highest values of U_*, *viz.*, 0.266 and 0.27 $\mathrm{m\,s^{-1}}$, are reported, there is no mention of any inversion.

The inversion heights reported by Yu are in multiples of 50 m, suggesting that the resolution of measurement was no higher; further it is stated that the "height of temperature inversion is likely to be a substantial overestimate". There seems to be no simple correlation between reported values of the inversion height and U_* as the former (not

surprisingly) also depends on the time of night at which the measurement was made. Also, there is no discussion by Yu about the influence of surface properties on inversion height, which can be substantial as the present study has shown. The simulation results discussed in the previous section show that for the highest values of U_* that we have used, *viz.* 0.5 $\mathrm{m\,s^{-1}}$ and 1 $\mathrm{m\,s^{-1}}$, the inversion is shallow and weak, and may even be non-existent. For lower values of U_*, *viz.* 0.1 and 0.2 $\mathrm{m\,s^{-1}}$, the inversion heights range from 30 m to about 45 m. In the light of the above discussion, the inversion heights obtained from the present simulation seem to be in qualitative agreement with the range of values reported by Yu. More quantitative comparisons cannot be made here as these would require more information on the site and the surface parameters than is available.

7. – Conclusions

The present simulations show that in the absence of eddy diffusion, that is when radiation alone is present, the evolution of the inversion height obeys the classical $\sqrt{t}$ law of Taylor [4], but only after a certain transient period. The onset of this parabolic growth is somewhat delayed when ground conductivity is small and so surface cooling is fast, and even more so when ground emissivity approaches unity. On the other hand, the onset of parabolic growth for the temperature differences ΔT_g or ΔT_s occurs much earlier at high ground cooling rates; the effect of ground emissivity on onset time seems weak.

It is found that the inversion height can be relatively high during calm conditions, being higher by about 40% when β is increased from 2 to 10 $\mathrm{K\,h^{-1/2}}$ or when ϵ_g is decreased from 1.0 to 0.7. Similarly, the temperature differences across the inversion are shown to vary substantially with ϵ_g and β. This dependence of the inversion parameters on ground emissivity and cooling rate has not been reported so far in the literature. From the results obtained in the present study, it can be emphatically stated that at least under conditions where radiation dominates, surface parameters have a significant influence on inversion characteristics and hence this influence ought to be taken into account where inversions are sought to be predicted.

It is also found that eddy diffusion initially raises the inversion height above the value under calm conditions, but eventually lowers it, the cross-over time occurring earlier as diffusion increases. Comparison with some available observations shows that the simulation results are in qualitative agreement, and suggests that the high variability of the results reported in the literature on inversion parameters may be due to site-dependent surface characteristics whose influence has till now been generally ignored. More thorough observations for specified surface characteristics are necessary to verify some of the predictions made here.

The results reported here demonstrate that it is essential to take proper account of surface properties like emissivity and soil conductivity in modelling the evolution of the nocturnal boundary layer. A full prognostic code that does this effectively will be separately reported.

* * *

We are grateful for the support that this work has received from the Department of Science and Technology, Government of India. The work reported here forms part of the M. Sc. thesis of SR, submitted to the Aerospace Engineering Department of the Indian Institute of Science. We are grateful to Prof. A. Prabhu for his kind support of this project.

REFERENCES

[1] Garratt J. R., *The Atmospheric Boundary Layer* (Cambridge University Press, UK) 1992.
[2] Vasudeva Murthy A. S., Srinivasan J. and Narasimha R., *Philos. Trans. R. Soc. London*, **344** (1993) 183.
[3] Ragothaman S., Narasimha R. and Vasudeva Murthy A. S., *Nuovo Cimento C*, **24** (2001) 353.
[4] Taylor G.I., *Philos. Trans. R. Soc. London, Ser. A*, **215** (1915) 1.
[5] Surridge A. D., *Boundary-Layer Meteorol.*, **36** (1986) 295.
[6] Ragothaman S., *Numerical simulation of nocturnal temperature profiles*, Thesis (M.Sc), Department of Aerospace Engineering, Indian Institute of Science, Bangalore, 1996.
[7] Fleagle R. G. and Badgley F. I., *The Nocturnal Cold Layer*, Occasional Rep. No. 2, Univ. of Washington, Atmospheric Turbulence study (AT 45-1) (1952).
[8] Lettau H. H., *Boundary-Layer Meteorol.*, **17** (1979) 443.
[9] Oke T.R., *Q. J. R. Meteorol. Soc.*, **96** (1970) 14.
[10] Raschke K., *Met. Rundschau,* **10** (1957) 1.
[11] Jacobs A. F. G., van Boxel J. H. and Nieveen J., *Agric. For. Meterol.*, **82** (1996) 155.
[12] Nieuwstadt F. T. M., *J. Appl. Meteorol.*, **19** (1980) 1445.
[13] Garratt J. R. and Brost R. A., *J. Atmos. Sci.*, **38** (1981) 2730.
[14] Andre J. C. and Mahrt L., *J. Atmos. Sci.*, **39** (1982) 864.
[15] Mahrt L., Heald R. C., Lenschow D. H., Stankov B. B. and Toren I. B., *Boundary-Layer Meteorol.*, **17** (1979) 247.
[16] Brunt D., *Physical and Dynamical Meteorology* (Cambridge University Press) 1941, pp. 124-146.
[17] Kloppel M. G., Stilke G. and Wamser C., *Boundary-Layer Meteorol.*, **15** (1978) 135.
[18] Anfossi D., Bacci B. and Longhetto A., *Q. J. R. Metorol. Soc.*, **102** (1976) 173.
[19] Delage Y., *Q. J. R. Metorol. Soc.*, **100** (1974) 351.
[20] Brost R.A. and Wyngaard J.C., *J. Atmos. Sci.*, **35** (1978) 1427.
[21] Zeman O., *J. Atmos. Sci.*, **36** (1979) 792.
[22] Surridge A. D. and Swanpoel D.J., *Boundary-Layer Meteorol.*, **40** (1987) 87.
[23] Liou K.-N and Ou, *J. Atmos. Sci.*, **40** (1983) 214.
[24] Liou K.-N, *An Introduction to Atmospheric Radiation* (Academic Press, New York) 1980.
[25] Zdunkowski W. and Johnson F. G., *J. Appl. Meteorol.*, **4** (1965) 371.
[26] Kaimal J. C. and Finnigan J. J., *Atmospheric Boundary Layer-Flows* (Oxford University Press) 1994.
[27] Vasudeva Murthy A. S., Srinivasan J. and Narasimha R., Report 91 AS 1, Centre for Atmospheric Sciences, Bangalore, India 1991.
[28] Narasimha R. and Vasudeva Murthy A. S., *Boundary-Layer Meteorol.*, **76** (1995) 307.
[29] Saji V., Vasudeva Murthy A. S. and Narasimha R. *Proc. Intl. Radiation Symposium, St. Petersburg, 24-29 July, 2000*, edited by Liou and others.
[30] Piggin I. G. and Alley S. K., *Mausam*, **45** (1994) 243.
[31] Ramdas L. A., Technical Note No. 21, Ind. Met. Dept., 1945.
[32] Raschke K., *Proc. Indian Acad. Sci. A*, **39** (1954) 98.
[33] Yu T., *J. Appl. Meteorol.*, **17** (1978) 28.